Geophys. J. Int. (2004) **159,** 607–621 doi: 10.1111/j.1365-246X.2004.02280.x

The effect of seafloor topography on magnetotelluric fields: an analytical formulation confirmed with numerical results

K. Schwalenberg and R. N. Edwards

Department of Physics, University of Toronto, Canada. E-mail: katrin@physics.utoronto.ca

Accepted 2004 February 9. Received 2004 February 6; in original form 2002 December 13

SUMMARY

Magnetotelluric fields and impedances are distorted at undulating interfaces. An analytical formulation is presented to calculate magnetotelluric effects in the presence of a sinusoidal interface. In contrast to previous analytical approaches, this formulation is not based on perturbation theory. It is applicable to observations both on land and on the seafloor. Electric and magnetic fields, as well as apparent resistivities and phases, are calculated on the interface. The topographic distortion on land mainly influences the TM mode data where the electric field is perpendicular to the geological strike. Both the TM mode and the orthogonal TE mode data are distorted on the seafloor. Systematic parameter tests indicate which modes are independent of the period and the conductivity contrast, provided that the induction depths are large relative to the amplitude of the topography. The differing physics of the seafloor and land surface is illustrated by plotting current streamlines. For the land model, contour lines diverge below a hill and converge below a valley. For the seafloor model, electric currents mainly flow in the conductive sea water. Contour lines converge above a hill and diverge above a valley. Numerical results, derived from finite-element modelling, support the analytical solutions. Streamlines of the electric current, derived from a model for the Central Andes, illustrate the connection between a graphical display of electromagnetic fields and an algebraic sensitivity analysis of the magnetotelluric impedance tensor.

Key words: magnetotelluric, marine electromagnetic methods, seafloor topography.

1 INTRODUCTION

The problem of topographic distortion is of major interest in magnetotelluric modelling and interpretation. Data can be distorted when measurements are carried out on an undulating land surface or seafloor generating on occasions a misinterpretation of subsurface structure. When the topography is well known, it may be included in the data interpretation process. There exist two possible approaches. The topography may be incorporated directly into the Earth model, or its effects can be estimated and the data corrected prior to inversion.

The first approach is usually numerical and has been applied frequently by many authors. Topography is built into a discrete model or an *a priori* model and the subsequent forward or inverse problem can be solved. One popular algorithm to model topography is the two-dimensional (2-D) finite-element code by Wannamaker (1990), where the non-planar surface or seafloor is approximated by triangular elements (Wannamaker *et al.* 1986). Baba & Seama (2002) present a new technique to incorporate seafloor topography into 2-D and 3-D forward modelling by transforming variations in oceanic thickness into variations in electrical properties. Baba (2002) extends the technique to correct 3-D topographic effects in magnetotelluric (MT) data. Nolasco *et al.* (1998) proceed in a hybrid manner. They apply a thin-sheet approximation to remove the bathymetric effect from a MT data set as accurately as possible. The resulting modified data set is then used for the subsequent interpretation. Two major disadvantages occur from the thin-sheet approximation as already established by Baba & Seama (2002): only 1-D structures can be incorporated in the model beneath the sheet, which is a significant restriction in the possible Earth models, and the thin-sheet approximation has limitations at short periods where the approximation that the skin depth is large compared with the thickness of the sheet breaks down. Li and Booker (personal communication) employ the 2-D inversion code modified from Smith & Booker (1988). The code uses the finite-difference approximation of Aprea *et al.* (1997) which can handle discrete boundaries of arbitrary geometry. Inversion results for a model with topography on land and with a coastline show good agreement with the respective forward responses. Chouteau & Bouchard (1988) present a correction technique to reduce the topographic effect for 2-D numerical models. They assume that the topographically distorted electric field response is equal to a distortion tensor multiplied by the undistorted electric field response. This technique works for land data, but cannot be directly transferred to the seafloor. Another variant is the Rayleigh Fourier transform technique introduced by Jiracek *et al.* (1989). The technique is based on the assumption that on a rough surface the fields can be expressed as superposition

of outgoing plane waves. The topographically distorted fields can then be corrected by a tensor stripping method. The method has also only been tested for land models.

The second approach is analytical and is often an application of perturbation theory which limits the character of the interface to small changes from plane geometry and allows only a limited range of small conductivity contrasts. Scientific progress on this problem can be traced back at least to the 1960s and early 1970s (Mann 1964; Rikitake 1965; Geyer 1970). Hughes (1973) published an analytical formulation for a periodic interface based on a Fourier transform of the governing Helmholtz equations. He considered the ratio of the vertical to the horizontal magnetic field as a measure of subsurface distortion. The linear approximations he made limit the applicability of his solution to small conductivity variations ($\log \sigma_1/\log \sigma_2$: $-1/-3$) and moderate topography of the interface (amplitude/wavelength ratio: 1/30).

The incorporation of the topography in the discrete forward or *a priori* model using finite-element or finite-difference methods is straightforward, allows complicated structures and is less expensive to implement. A major disadvantage of the numerical approach is the generation of instabilities at large conductivity contrasts, typical of the interface between conductive sea water and resistive oceanic crust. Analytical approaches, on the other hand, generally apply to very simple models which might not represent reality but which provide exact results to verify numerical algorithms.

We present here an analytical formulation to calculate magnetotelluric fields for a harmonic surface both on land and on the seafloor following the method of Hughes (1973). However, our approach will not be restricted by the character of the topography or conductivity contrast. The theory leads implicitly to a double-series expansion and the determination of unknown coefficient from boundary equations. Unlike in Mann (1964) and Hughes (1973) there is no truncation of the series to first-order terms.

We present results calculated on the interface to verify our approach and discuss the different effects of topographic distortion on land and on the seafloor. We also show current streamlines which are contour lines of the magnetic field parallel to strike. Finally, we will compare these results with numerically derived fields using Wannamaker's 2-D code (Wannamaker 1990). A discrete model with the same properties as the analytical model will be applied. The illustration of current streamlines is instructive, so we also present them for a discrete coast model and a resistivity model derived from a data set from the Central Andes.

2 THEORY

The basic model is a sinusoidal interface as shown in Fig. 1. The Cartesian coordinate system has x normal to strike, y along strike and z positive downwards. The upper and lower regions have conductivities σ_1 and σ_2 respectively. The topography on the interface is 2-D, harmonic and defined by the equation $z = \Delta\cos(\nu x)$ where Δ and ν are the amplitude and wavenumber respectively.

We shall present the formulation for the TM mode, in which the single component of the magnetic field is parallel to strike, and then the corresponding solution of the TE mode, in which the single component of the electric field is parallel to strike.

2.1 TM mode

We can write the damped wave equation for the magnetic field B_y parallel to strike as

$$\frac{\partial^2 B_y}{\partial x^2} + \frac{\partial^2 B_y}{\partial z^2} = \left(i\omega\mu_0\sigma - \omega^2\mu_0\epsilon\right) B_y \tag{1}$$

where ω is the angular frequency, μ_0 is the permeability of free space and ϵ is the dielectric constant of the region. A solution in series for eq. (1) is

$$B_y(x, z) = \sum_{n=0}^{\infty} B_n(z)\cos(n\nu x) \tag{2}$$

where the set $n\nu$ describes the harmonics of the secondary fields generated by the interface. The coefficients B_n satisfy the equation

$$\frac{d^2 B_n}{dz^2} - \theta_n^2 B_n = 0, \tag{3}$$

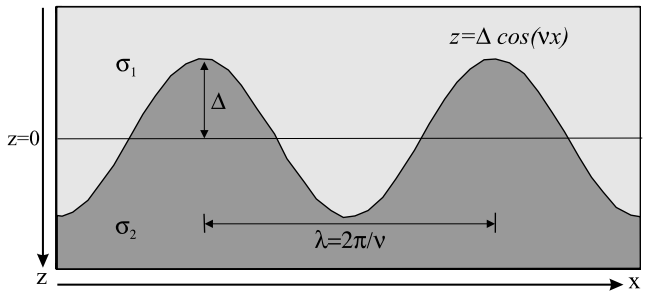

Figure 1. The basic model for the analytical formulation is an interface described by a cosine with wavelength λ and amplitude Δ which separates an upper region with conductivity σ_1 from a lower region with conductivity σ_2. z is positive downwards.

with $\theta_n = \sqrt{i\omega\mu_0\sigma - \omega^2\mu_0\epsilon + n^2\nu^2}$. The conductivity is zero in the air beneath any source currents. For typical values of ω, $\nu^2 \gg \omega^2\mu_0\epsilon_0$ so that only $\theta_n^2 = n^2\nu^2$ is retained in the differential equation. We can neglect the magnetic effects of displacement currents in the Earth or below the sea surface where $\sigma \gg \omega\epsilon$, and θ_n reduces to $\sqrt{i\omega\mu_0\sigma + n^2\nu^2}$. The differential eq. (3) has exponential solutions of the form

$$B_n(z) = \alpha_n e^{\theta_n z} + \beta_n e^{-\theta_n z}. \tag{4}$$

The first and second terms on the right-hand side describe downward- and upward-diffusing fields respectively. The unknown coefficients α_n and β_n are determined from boundary conditions. The two components E_x and E_z of the electric fields are given by Maxwell's equations as

$$E_x = -\frac{1}{\mu_0\sigma}\frac{\partial B_y}{\partial z} \tag{5}$$

and

$$E_z = \frac{1}{\mu_0\sigma}\frac{\partial B_y}{\partial x}. \tag{6}$$

2.1.1 Boundary conditions, TM mode

The magnetic field that excites the interface diffuses downwards through region 1 and has the simple form of

$$B_0 e^{-\theta_0^1 z} \tag{7}$$

where B_0 is a constant source term which we set to 1 for simplicity. The magnetic field scattered upwards into region 1 from the interface is

$$\sum_{n=0}^{\infty} \beta_n e^{\theta_n^1 z}\cos(n\nu x), \tag{8}$$

while the magnetic field scattered downwards into region 2 from the interface is

$$\sum_{n=0}^{\infty} \gamma_n e^{-\theta_n^2 z}\cos(n\nu x). \tag{9}$$

The convention we use to define θ in the upper and lower regions is $(\theta_n^1)^2 = i\omega\mu_0\sigma_1 + n^2\nu^2$ and $(\theta_n^2)^2 = i\omega\mu_0\sigma_2 + n^2\nu^2$ respectively. The magnetic field is continuous across the interface so that

$$B_y : B_0 e^{-\theta_0^1 \Delta\cos(\nu x)} + \sum_{n=0}^{\infty} \beta_n e^{\theta_n^1 \Delta\cos(\nu x)}\cos(n\nu x) = \sum_{n=0}^{\infty} \gamma_n e^{-\theta_n^2 \Delta\cos(\nu x)}\cos(n\nu x). \tag{10}$$

For the TM mode magnetic field there exists an alternative way to formulate the boundary conditions on a land surface where σ_1 is negligible compared with σ_2. It can be shown that the magnetic field on the Earth's surface parallel to strike is a constant and only depends on the source field. On the interface we may use

$$B_1 = \sum_{n=0}^{\infty} \gamma_n e^{-\theta_n^2 \Delta\cos(\nu x)}\cos(n\nu x) \tag{11}$$

instead of eq. (10). In this case we have to solve only for one set of unknown coefficients (γ_n). Both eqs (10) and (11) lead to the same result that $B_1 = 2B_0$.

The tangential component of the electric field E_t is also continuous across the interface. It is the linear combination of E_x and E_z:

$$E_t = E_x\cos\psi + E_z\sin\psi. \tag{12}$$

The angle ψ may be calculated from the slope of the interface and is given by $\psi = \arctan[-\nu\Delta\sin(\nu x)]$.

In regions 1 and 2 the components of the electric fields are derived from eqs (5) and (6) as

$$E_x^1 : \frac{1}{\mu_0\sigma_1}\theta_0^1 B_0 e^{-\theta_0^1 \Delta\cos(\nu x)} - \frac{1}{\mu_0\sigma_1}\sum_{n=0}^{\infty} \theta_n^1\beta_n e^{\theta_n^1 \Delta\cos(\nu x)}\cos(n\nu x); \tag{13}$$

$$E_x^2 : \frac{1}{\mu_0\sigma_2}\sum_{n=0}^{\infty} \theta_n^2\gamma_n e^{-\theta_n^2 \Delta\cos(\nu x)}\cos(n\nu x); \tag{14}$$

$$E_z^1 : \frac{1}{\mu_0\sigma_1}\theta_0^1\Delta\nu\sin(\nu x)\, B_0 e^{-\theta_0^1\Delta\cos(\nu x)} - \frac{1}{\mu_0\sigma_1}\left(\sum_{n=0}^{\infty}\theta_n^1\beta_n\Delta\nu\sin(\nu x)\cdot e^{\theta_n^1\Delta\cos(\nu x)}\cdot\cos(n\nu x) + \sum_{n=0}^{\infty} n\nu\beta_n\cdot e^{\theta_n^1\Delta\cos(\nu x)}\cdot\sin(n\nu x)\right); \tag{15}$$

$$E_z^2 : \frac{1}{\mu_0\sigma_2}\left(\sum_{n=0}^{\infty}\theta_n^2\gamma_n\Delta\nu\sin(\nu x)\cdot e^{-\theta_n^2\Delta\cos(\nu x)}\cdot\cos(n\nu x) - \sum_{n=0}^{\infty} n\nu\gamma_n\cdot e^{-\theta_n^2\Delta\cos(\nu x)}\cdot\sin(n\nu x)\right). \tag{16}$$

2.1.2 Expansion as modified Bessel functions, TM mode

Two useful expansions are

$$e^{\theta_n \Delta \cos(\nu x)} = \sum_{k=0}^{\infty} (2 - \delta_{0k}) I_k(\theta_n \Delta) \cos(k\nu x); \tag{17}$$

$$e^{-\theta_n \Delta \cos(\nu x)} = \sum_{k=0}^{\infty} (-1)^k (2 - \delta_{0k}) I_k(\theta_n \Delta) \cos(k\nu x) \tag{18}$$

(Gradshteyn & Ryzhik 2000, eqs 8.406.3, 8.511.3 and 8.511.4) where I_k are modified Bessel functions and δ_{0k} is the Kronecker delta. We apply eqs (17) and (18) to the expressions for the magnetic field in eq. (10) and for the electric field components in eqs (13–16). In doing so we also use the following trigonometric products:

$$\cos a \cos b = 1/2[\cos(a + b) + \cos(\pm(a - b))]; \tag{19}$$

$$\cos a \sin b = \begin{cases} 1/2[\sin(a + b) - \sin(a - b)] \\ 1/2[\sin(a + b) + \sin(b - a)]. \end{cases} \tag{20}$$

The boundary condition for the magnetic field on the interface leads to

$$\begin{aligned} B_y : B_0 &\sum_{k=0}^{\infty} (-1)^k (2 - \delta_{0k}) I_k \left(\theta_0^1 \Delta\right) \cos(k\nu x) \\ &+ \sum_{n=0}^{\infty} \beta_n \sum_{k=0}^{\infty} (1 - 1/2\delta_{0k}) I_k \left(\theta_n^1 \Delta\right) \{\cos[(n + k)\nu x] + \cos[(n - k)\nu x]\} \\ &= \sum_{n=0}^{\infty} \gamma_n \sum_{k=0}^{\infty} (-1)^k (1 - 1/2\delta_{0k}) I_k \left(\theta_n^2 \Delta\right) \{\cos[(n + k)\nu x] + \cos[(n - k)\nu x]\} \end{aligned} \tag{21}$$

and for the electric field components we obtain

$$\begin{aligned} E_x^1 : \frac{\theta_0^1}{\mu_0 \sigma_1} B_0 &\sum_{k=0}^{\infty} (-1)^k (2 - \delta_{0k}) I_k(\theta_0^1 \Delta) \cos(k\nu x) \\ &- \sum_{n=0}^{\infty} \frac{\theta_n^1}{\mu_0 \sigma_1} \beta_n \sum_{k=0}^{\infty} (1 - 1/2\delta_{0k}) I_k(\theta_n^1 \Delta) \{\cos[(n + k)\nu x] + \cos[(n - k)\nu x]\}; \end{aligned} \tag{22}$$

$$E_x^2 : \sum_{n=0}^{\infty} \frac{\theta_n^2}{\mu_0 \sigma_2} \gamma_n \sum_{k=0}^{\infty} (-1)^k (1 - 1/2\delta_{0k}) I_k \left(\theta_n^2 \Delta\right) \{\cos[(n + k)\nu x] + \cos[(n - k)\nu x]; \tag{23}$$

$$\begin{aligned} E_z^1 : \frac{1}{\mu_0 \sigma_1} \theta_0^1 \Delta \nu \sin(\nu x) B_0 &\sum_{k=0}^{\infty} (-1)^k (2 - \delta_{0k}) I_k \left(\theta_0^1 \Delta\right) \cos(k\nu x) \\ - \frac{1}{\mu_0 \sigma_1} &\sum_{n=0}^{\infty} \theta_n^1 \beta_n \Delta \nu \sin(\nu x) \sum_{k=0}^{\infty} (1 - 1/2\delta_{0k}) I_k \left(\theta_n^1 \Delta\right) \{\cos[(n + k)\nu x] + \cos[(n - k)\nu x]\} \\ - \frac{1}{\mu_0 \sigma_1} &\sum_{n=0}^{\infty} n\nu \beta_n \sum_{k=0}^{\infty} (1 - 1/2\delta_{0k}) I_k \left(\theta_n^1 \Delta\right) \begin{bmatrix} \sin[(n + k)\nu x] & + \sin[(n - k)\nu x] \\ & - \sin[(k - n)\nu x] \end{bmatrix}; \end{aligned} \tag{24}$$

$$\begin{aligned} E_z^2 : \frac{1}{\mu_0 \sigma_2} &\sum_{n=0}^{\infty} \theta_n^2 \gamma_n \Delta \nu \sin(\nu x) \sum_{k=0}^{\infty} (-1)^k (1 - 1/2\delta_{0k}) I_k \left(\theta_n^2 \Delta\right) \{\cos[(n + k)\nu x] + \cos[(n - k)\nu x]\} \\ - \frac{1}{\mu_0 \sigma_2} &\sum_{n=0}^{\infty} n\nu \gamma_n \sum_{k=0}^{\infty} (-1)^k (1 - 1/2\delta_{0k}) I_k \left(\theta_n^2 \Delta\right) \begin{bmatrix} \sin[(n + k)\nu x] & + \sin[(n - k)\nu x] \\ & - \sin[(k - n)\nu x] \end{bmatrix}. \end{aligned} \tag{25}$$

The next step is to collect coefficients of the orthogonal harmonics. Zhdanov & Keller (1994) point out that the process 'results in a good deal of tedious algebra'. We simplify the analysis by neglecting the contributions of the vertical electric field to the tangential electric field which is reasonable for realistic topography (amplitude/wavelength ratio ~1/10), and require instead that the horizontal electric field is continuous across the interface ($E_x^1 = E_x^2$).

Sorting the resulting series in order of $\cos(n\nu x)$ and rearranging the equations so that the right-hand side only depends on the source term and the left-hand side contains the coefficients β_n and γ_n finally leads to a system of linear equations $Ax = b$ with $2n$ equations for the $2n$ unknown coefficients. In Fig. 2 (top) we present the equation system for the TM mode for $n = (0, 1, 2)$. The compilation of the linear equation system is a significant result. In practice it can be calculated for any order of n.

The coefficients β_n and γ_n can be obtained by inverting the equation system. The magnetic and electric field quantities for the upper (B_y^1, E_x^1) and lower region on the interface (B_y^2, E_x^2) can be calculated from eqs (10), (13) and (14). To calculate the fields anywhere else in the

TM-Mode

$$\begin{bmatrix}
+I_0^1(\theta_0^1\Delta) & -I_0^2(\theta_0^2\Delta) & +I_1^1(\theta_1^1\Delta) & +I_1^2(\theta_1^2\Delta) & +0 & -0 \\
-\frac{\theta_0^1}{\mu_0\sigma_1}I_0^1(\theta_0^1\Delta) & -\frac{\theta_0^2}{\mu_0\sigma_2}I_0^2(\theta_0^2\Delta) & -\frac{\theta_1^1}{\mu_0\sigma_1}I_1^1(\theta_1^1\Delta) & +\frac{\theta_1^2}{\mu_0\sigma_2}I_1^2(\theta_1^2\Delta) & -0 & -0 \\
+2I_1^1(\theta_0^1\Delta) & +2I_1^2(\theta_0^2\Delta) & +\left(I_0^1(\theta_1^1\Delta)+I_2^1(\theta_1^1\Delta)\right) & -\left(I_0^2(\theta_1^2\Delta)+I_2^2(\theta_1^2\Delta)\right) & +I_1^1(\theta_2^1\Delta) & +I_1^2(\theta_2^2\Delta) \\
-2\frac{\theta_0^1}{\mu_0\sigma_1}I_1^1(\theta_0^1\Delta) & +2\frac{\theta_0^2}{\mu_0\sigma_2}I_1^2(\theta_0^2\Delta) & -\frac{\theta_1^1}{\mu_0\sigma_1}\left(I_0^1(\theta_1^1\Delta)+I_2^1(\theta_1^1\Delta)\right) & -\frac{\theta_1^2}{\mu_0\sigma_2}\left(I_0^2(\theta_1^2\Delta)+I_2^2(\theta_1^2\Delta)\right) & -\frac{\theta_2^1}{\mu_0\sigma_1}I_1^1(\theta_2^1\Delta) & +\frac{\theta_2^2}{\mu_0\sigma_2}I_1^2(\theta_2^2\Delta) \\
+2I_2^1(\theta_0^1\Delta) & -2I_2^2(\theta_0^2\Delta) & +\left(I_1^1(\theta_1^1\Delta)+I_3^1(\theta_1^1\Delta)\right) & +\left(I_1^2(\theta_1^2\Delta)+I_3^2(\theta_1^2\Delta)\right) & +\left(I_0^1(\theta_2^1\Delta)+I_2^1(\theta_2^1\Delta)\right) & -\left(I_0^2(\theta_2^2\Delta)+I_2^2(\theta_2^2\Delta)\right) \\
-2\frac{\theta_0^1}{\mu_0\sigma_1}I_2^1(\theta_0^1\Delta) & -2\frac{\theta_0^2}{\mu_0\sigma_2}I_2^2(\theta_0^2\Delta) & -\frac{\theta_1^1}{\mu_0\sigma_1}\left(I_1^1(\theta_1^1\Delta)+I_3^1(\theta_1^1\Delta)\right) & +\frac{\theta_1^2}{\mu_0\sigma_2}\left(I_1^2(\theta_1^2\Delta)+I_3^2(\theta_1^2\Delta)\right) & -\frac{\theta_2^1}{\mu_0\sigma_1}\left(I_0^1(\theta_2^1\Delta)+I_2^1(\theta_2^1\Delta)\right) & -\frac{\theta_2^2}{\mu_0\sigma_2}\left(I_0^2(\theta_2^2\Delta)+I_2^2(\theta_2^2\Delta)\right)
\end{bmatrix}\cdot\begin{bmatrix}\beta_0\\ \gamma_0\\ \beta_1\\ \gamma_1\\ \beta_2\\ \gamma_2\end{bmatrix}=\begin{bmatrix}
-B_0I_0^1(\theta_0^1\Delta) \\
-\frac{\theta_0^1}{\mu_0\sigma_1}B_0I_0^1(\theta_0^1\Delta) \\
+2B_0I_1^1(\theta_0^1\Delta) \\
+2\frac{\theta_0^1}{\mu_0\sigma_1}B_0I_1^1(\theta_0^1\Delta) \\
-2B_0I_2^1(\theta_0^1\Delta) \\
-2\frac{\theta_0^1}{\mu_0\sigma_1}B_0I_2^1(\theta_0^1\Delta)
\end{bmatrix}$$

TE-Mode

$$\begin{bmatrix}
+I_0^1(\theta_0^1\Delta) & -I_0^2(\theta_0^2\Delta) & +I_1^1(\theta_1^1\Delta) & +I_1^2(\theta_1^2\Delta) & +0 & -0 \\
+\frac{\theta_0^1}{i\omega}I_0^1(\theta_0^1\Delta) & +\frac{\theta_0^2}{i\omega}I_0^2(\theta_0^2\Delta) & +\frac{\theta_1^1}{i\omega}I_1^1(\theta_1^1\Delta) & -\frac{\theta_1^2}{i\omega}I_1^2(\theta_1^2\Delta) & +0 & +0 \\
+2I_1^1(\theta_0^1\Delta) & +2I_1^2(\theta_0^2\Delta) & +\left(I_0^1(\theta_1^1\Delta)+I_2^1(\theta_1^1\Delta)\right) & -\left(I_0^2(\theta_1^2\Delta)+I_2^2(\theta_1^2\Delta)\right) & +I_1^1(\theta_2^1\Delta) & +I_1^2(\theta_2^2\Delta) \\
+2\frac{\theta_0^1}{i\omega}I_1^1(\theta_0^1\Delta) & -2\frac{\theta_0^2}{i\omega}I_1^2(\theta_0^2\Delta) & +\frac{\theta_1^1}{i\omega}\left(I_0^1(\theta_1^1\Delta)+I_2^1(\theta_1^1\Delta)\right) & +\frac{\theta_1^2}{i\omega}\left(I_0^2(\theta_1^2\Delta)+I_2^2(\theta_1^2\Delta)\right) & +\frac{\theta_2^1}{\mu_0\sigma_1}I_1^1(\theta_2^1\Delta) & -\frac{\theta_2^2}{i\omega}I_1^2(\theta_2^2\Delta) \\
+2I_2^1(\theta_0^1\Delta) & -2I_2^2(\theta_0^2\Delta) & +\left(I_1^1(\theta_1^1\Delta)+I_3^1(\theta_1^1\Delta)\right) & +\left(I_1^2(\theta_1^2\Delta)+I_3^2(\theta_1^2\Delta)\right) & +\left(I_0^1(\theta_2^1\Delta)+I_2^1(\theta_2^1\Delta)\right) & -\left(I_0^2(\theta_2^2\Delta)+I_2^2(\theta_2^2\Delta)\right) \\
+2\frac{\theta_0^1}{i\omega}I_2^1(\theta_0^1\Delta) & +2\frac{\theta_0^2}{i\omega}I_2^2(\theta_0^2\Delta) & +\frac{\theta_1^1}{i\omega}\left(I_1^1(\theta_1^1\Delta)+I_3^1(\theta_1^1\Delta)\right) & -\frac{\theta_1^2}{i\omega}\left(I_1^2(\theta_1^2\Delta)+I_3^2(\theta_1^2\Delta)\right) & +\frac{\theta_2^1}{\mu_0\sigma_1}\left(I_0^1(\theta_2^1\Delta)+I_2^1(\theta_2^1\Delta)\right) & +\frac{\theta_2^2}{i\omega}\left(I_0^2(\theta_2^2\Delta)+I_2^2(\theta_2^2\Delta)\right)
\end{bmatrix}\cdot\begin{bmatrix}\beta_0\\ \gamma_0\\ \beta_1\\ \gamma_1\\ \beta_2\\ \gamma_2\end{bmatrix}=\begin{bmatrix}
-E_0I_0^1(\theta_0^1\Delta) \\
+\frac{\theta_0^1}{i\omega}E_0I_0^1(\theta_0^1\Delta) \\
+2E_0I_1^1(\theta_0^1\Delta) \\
-2\frac{\theta_0^1}{i\omega}E_0I_1^1(\theta_0^1\Delta) \\
-2E_0I_2^1(\theta_0^1\Delta) \\
+2\frac{\theta_0^1}{i\omega}E_0I_2^1(\theta_0^1\Delta)
\end{bmatrix}$$

Figure 2. Compilation of the linear equation system to solve for the unknown coefficients β_n and γ_n for the TM mode (top) and the TE mode (bottom), both for orders $n = 0, 1, 2$. The convention we use to define θ in the upper and lower regions is $(\theta_n^1)^2 = i\omega\mu_0\sigma_1 + n^2\nu^2$ and $(\theta_n^2)^2 = i\omega\mu_0\sigma_2 + n^2\nu^2$ respectively.

model, we use

$$B_y^1 : B_0 e^{-\theta_0^1 z} + \sum_{n=0}^{\infty} \beta_n e^{\theta_n^1 z} \cos(n\nu x); \tag{26}$$

$$E_x^1 : \frac{1}{\mu_0\sigma_1}\theta_0^1 B_0 e^{-\theta_0^1 z} - \frac{1}{\mu_0\sigma_1}\sum_{n=0}^{\infty} \theta_n^1 \beta_n e^{\theta_n^1 z} \cos(n\nu x) \tag{27}$$

above the interface and

$$B_y^2 : \sum_{n=0}^{\infty} \gamma_n e^{-\theta_n^2 z} \cos(n\nu x); \tag{28}$$

$$E_x^2 : \frac{1}{\mu_0\sigma_2}\sum_{n=0}^{\infty} \theta_n^2 \gamma_n e^{-\theta_n^2 z} \cos(n\nu x) \tag{29}$$

below the interface.

2.2 TE mode

The analysis for the TE mode is similar to the TM mode formulation. The damped wave equation for the electric field E_y parallel to strike is

$$\frac{\partial^2 E_y}{\partial x^2} + \frac{\partial^2 E_y}{\partial z^2} = \left(i\omega\mu_0\sigma - \omega^2\mu_0\epsilon\right)E_y. \tag{30}$$

An expansion in series for E_y is given by

$$E_y(x, z) = \sum_{n=0}^{\infty} E_n(z)\cos(n\nu x) \tag{31}$$

where the coefficients E_n satisfy the equation

$$\frac{d^2 E_n}{dz^2} - \theta_n^2 E_n = 0 \tag{32}$$

with $\theta_n = \sqrt{i\omega\mu_0\sigma - \omega^2\mu_0\epsilon + n^2\nu^2}$. Neglecting the effects of displacement currents, θ_n reduces to $\sqrt{i\omega\mu_0\sigma + n^2\nu^2}$ in the Earth or below the sea surface and to $\sqrt{n^2\nu^2}$ in the air where $\sigma \approx 0$. An exponential approach to solve for $E_n(z)$ in eq. (32) is given by

$$E_n(z) = \alpha_n e^{\theta_n z} + \beta_n e^{-\theta_n z} \tag{33}$$

where the first and second terms on the right-hand side refer to downward and upward diffusing fields. The unknown coefficients α_n and β_n are derived from boundary conditions. Therefore we also need the components of the magnetic field B_x and B_z which we derive from Maxwell's equations as

$$B_x = \frac{1}{i\omega}\frac{\partial E_y}{\partial z}, \tag{34}$$

$$B_z = -\frac{1}{i\omega}\frac{\partial E_y}{\partial x}. \tag{35}$$

2.2.1 Boundary conditions, TE mode

In the TE mode case, the exciting field is the electric field that diffuses downward through region 1. At the interface, it excites an electric field scattered upwards into region 1 from the interface and an electric field scattered downwards into region 2 from the interface. In the TE mode case, the tangential component of the electric field is always parallel to strike and continuous across the interface so that

$$E_y : E_0 \mathrm{e}^{-\theta_0^1 \Delta \cos(\nu x)} + \sum_{n=0}^{\infty} \beta_n \mathrm{e}^{\theta_n^1 \Delta \cos(\nu x)} \cos(n\nu x) = \sum_{n=0}^{\infty} \gamma_n \mathrm{e}^{-\theta_n^2 \Delta \cos(\nu x)} \cos(n\nu x). \tag{36}$$

E_0 is a constant source term. We will use the same variables for the unknown coefficients β_n and γ_n as in the TM mode formulation. According to the boundary conditions all components of the magnetic field are continuous on the interface. It is therefore sufficient if we only consider the horizontal magnetic fields in the upper and lower region (B_x^1, B_x^2) which we derive from eq. (34).

$$B_x : -\frac{1}{i\omega}\theta_0^1 E_0 \mathrm{e}^{-\theta_0^1 \Delta \cos(\nu x)} + \frac{1}{i\omega}\sum_{n=0}^{\infty} \theta_n^1 \beta_n \mathrm{e}^{\theta_n^1 \Delta \cos(\nu x)} \cos(n\nu x) = -\frac{1}{i\omega}\sum_{n=0}^{\infty} \theta_n^2 \gamma_n \mathrm{e}^{-\theta_n^2 \Delta \cos(\nu x)} \cos(n\nu x). \tag{37}$$

2.2.2 Expansion as modified Bessel functions, TE mode

To solve for the unknown coefficients β_n and γ_n, we apply the expansions of modified Bessel functions in eqs (17) and (18), and use eq. (19). For the electric field in eq. (36) we obtain

$$\begin{aligned} E_y : {} & E_0 \sum_{k=0}^{\infty} (-1)^k (2 - \delta_{0k}) I_k\left(\theta_0^1 \Delta\right) \cos(k\nu x) \\ & - \sum_{n=0}^{\infty} \beta_n \sum_{k=0}^{\infty} (1 - 1/2\delta_{0k}) I_k\left(\theta_n^1 \Delta\right) \{\cos[(n+k)\nu x] + \cos[(n-k)\nu x]\} \\ & = \sum_{n=0}^{\infty} \gamma_n \sum_{k=0}^{\infty} (-1)^k (1 - 1/2\delta_{0k}) I_k\left(\theta_n^2 \Delta\right) \{\cos[(n+k)\nu x] + \cos[(n-k)\nu x]\} \end{aligned} \tag{38}$$

and for the TE mode magnetic field in eq. (37) follows

$$\begin{aligned} B_x : {} & -\frac{\theta_0^1}{i\omega} E_0 \sum_{k=0}^{\infty} (-1)^k (2 - \delta_{0k}) I_k\left(\theta_0^1 \Delta\right) \cos(k\nu x) \\ & + \sum_{n=0}^{\infty} \frac{\theta_n^1}{i\omega} \beta_n \sum_{k=0}^{\infty} (1 - 1/2\delta_{0k}) I_k\left(\theta_n^1 \Delta\right) \{\cos[(n+k)\nu x] + \cos[(n-k)\nu x]\} \\ & = -\sum_{n=0}^{\infty} \frac{\theta_1^2}{i\omega} \gamma_n \sum_{k=0}^{\infty} (-1)^k (1 - 1/2\delta_{0k}) I_k\left(\theta_n^2 \Delta\right) \{\cos[(n+k)\nu x] + \cos[(n-k)\nu x]\}. \end{aligned} \tag{39}$$

In analogy to the TM mode we expand these two equations into a series of orders n and k, sort these series for orders of $\cos(n\nu x)$ and bring the source terms to the right-hand side. The outcome of this is a system of linear equations $Ax = b$ for the TE mode. For $n = (0, 1, 2)$ this is shown in Fig. 2 (bottom). As before, the unknown coefficients β_n and γ_n can be calculated by simply inverting the equation system. Electric and magnetic field quantities for the TE mode on the interface are now provided by eqs (36) and (37) and for the entire model by

$$E_y^1 : E_0 \mathrm{e}^{-\theta_0^1 z} + \sum_{n=0}^{\infty} \beta_n \mathrm{e}^{\theta_n^1 z} \cos(n\nu x); \tag{40}$$

$$B_x^1 : -\frac{1}{i\omega}\theta_0^1 E_0 \mathrm{e}^{-\theta_0^1 z} + \frac{1}{i\omega}\sum_{n=0}^{\infty} \theta_n^1 \beta_n \mathrm{e}^{\theta_n^1 z} \cos(n\nu x) \tag{41}$$

above the interface and

$$E_y^2 : \sum_{n=0}^{\infty} \gamma_n \mathrm{e}^{-\theta_n^2 z} \cos(n\nu x); \tag{42}$$

$$B_x^2 : -\frac{1}{i\omega}\sum_{n=0}^{\infty} \theta_n^2 \gamma_n \mathrm{e}^{-\theta_n^2 z} \cos(n\nu x) \tag{43}$$

below the interface.

Table 1. Input parameters for the standard model.

Conductivities	$\sigma_1 = 10^{-10}$ S m^{-1} air, $\sigma_2 = 0.01$ S m^{-1} crust
	$\sigma_1 = 3$ S m^{-1} sea water
Period	$T = 100$ s
Amplitude	$\Delta = 100$ m
Wavelength	$\lambda = 1000$ m
Source terms	$B_0 = 1$, $E_0 = 1$
Orders in (ν x)	$n = 10$

3 ANALYTICAL RESULTS

In the preceding section we derived a scheme to calculate TM and TE mode magnetotelluric data in the presence of a harmonic interface. The approach applies to both seafloor and land models. We compiled MATLAB routines to calculate all field quantities. The parameters for the standard seafloor and land model are listed in Table 1. All quantities can be calculated at arbitrary (x, z) values.

3.1 Results on the interface

3.1.1 Electric and magnetic fields

To begin with, we present results calculated on the interface. In Fig. 3, electric and magnetic fields are shown for a sinusoidal land surface (left panels) and a sinusoidal seafloor (right panels). All fields are normalized by the respective field quantities calculated for a flat interface, thus the fields are of the same order of magnitude. TM mode magnetic and electric fields are obtained from eq. (10), and eqs (13) and (14) respectively. TE mode electric and magnetic fields are derived from eqs (36) and (37). The boundary conditions apply for both the land surface and the seafloor model. The field responses for the upper region (black lines) and for the lower region (grey lines) agree on the interface with the exception of the TM mode magnetic fields on the seafloor where deviations are maximal when the slope of the interface is maximum, and minimal when the slope is zero.

On land, topographic distortion occurs only in the TM mode electric fields. The TM mode magnetic fields are not affected. They only depend on the source field and do not carry information about the subsurface (Jegen 1997). The TE mode fields are not affected by topography.

On the seafloor, topographic distortion occurs in the TM mode electric fields and the TE mode magnetic fields. The TM mode electric fields are asymmetrically distorted on land and on the seafloor, but in an opposite manner: While the electric fields are decreased when measurements are carried out on a hill on land, they are increased above a seafloor elevation. The TM mode magnetic fields are constantly reduced by the sea water.

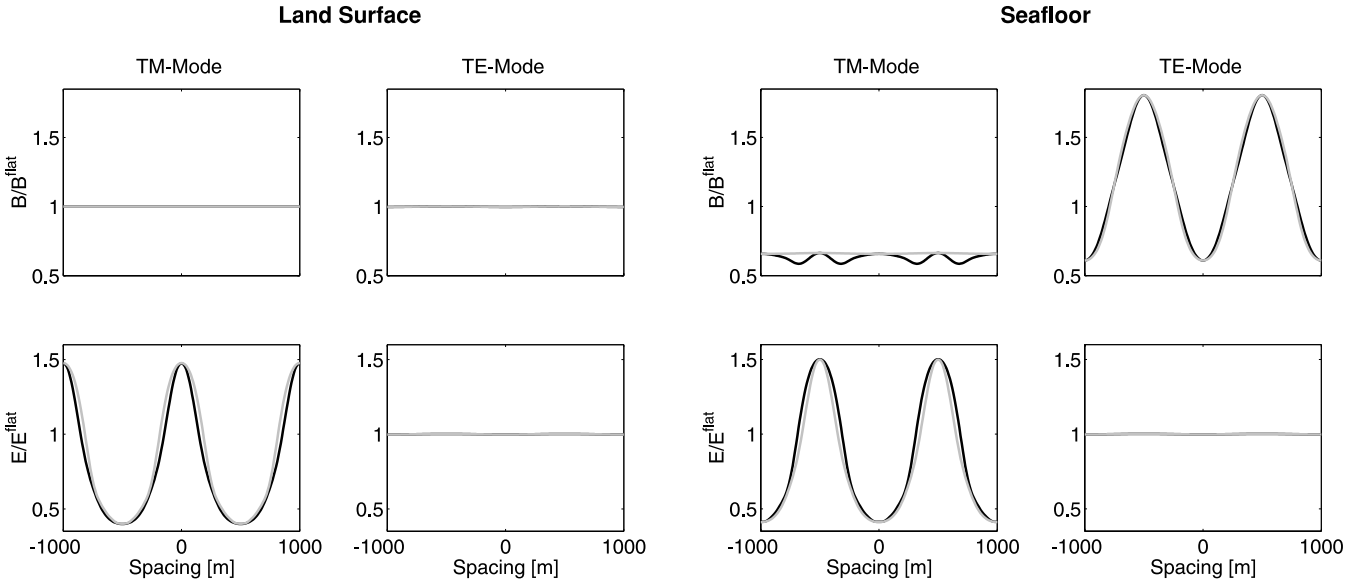

Figure 3. Magnetic and electric fields calculated for a sinusoidal land surface (left) and a sinusoidal seafloor (right). The quantities are normalized by their respective field values derived from a flat interface. Normalized fields in the upper region (black line) and in the lower region (grey line) agree on the interface thus demonstrating the validity of the analytical formulation. On land, only the TM mode electric field is affected by topography. On the seafloor, the TM mode electric fields and the TE mode magnetic fields are distorted by the topography. The TM mode magnetic field is constantly reduced by the sea water.

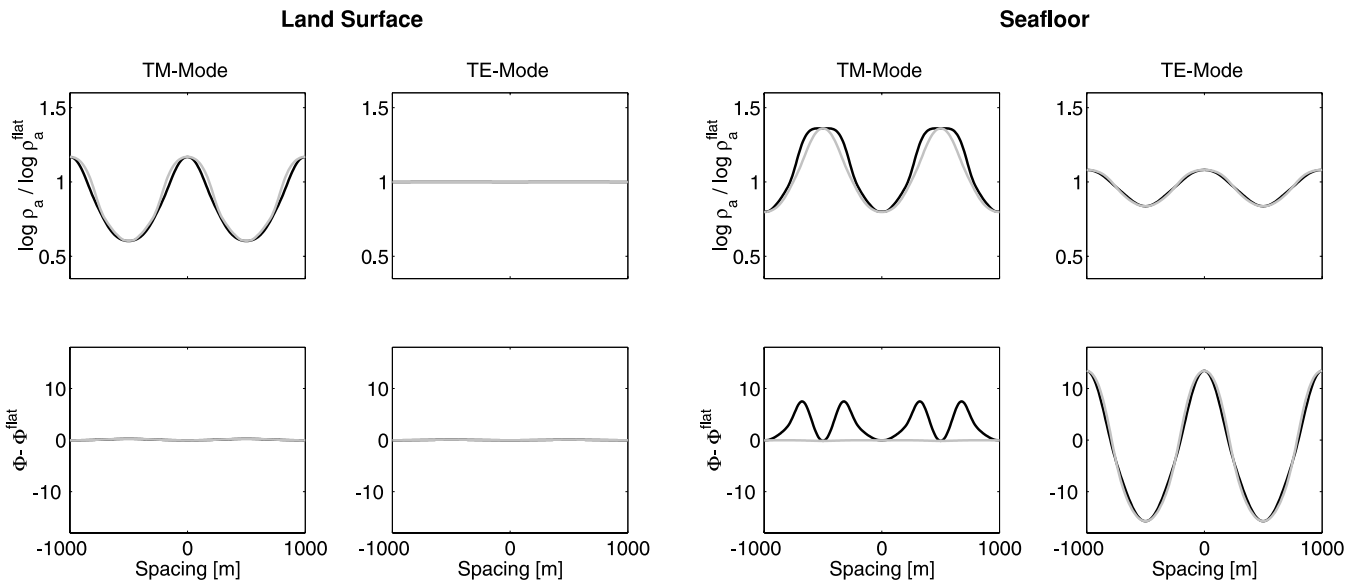

Figure 4. Normalized apparent resistivities and phases have been calculated for the upper region (black lines) and the lower region (grey lines). Solutions from both regions match on the interface and thus fulfil the boundary conditions with the exception of the TM mode phases on the seafloor. On land, topographic distortion only appears in the TM mode. On the seafloor, both modes are affected. Apparent resistivities show the opposite behaviour to that observed on land.

3.1.2 Apparent resistivities and phases

From the electric and magnetic fields we can now calculate apparent resistivities and phases. The magnetotelluric impedance Z is defined by

$$Z = E/B \tag{44}$$

and the apparent resistivity ρ_a and phase φ by

$$\begin{aligned} \rho_a &= \mu_0/\omega|Z|^2; \\ \varphi &= \arctan(\mathrm{Im}Z/\mathrm{Re}Z). \end{aligned} \tag{45}$$

In Fig. 4, we show apparent resistivities (top row) and phases (bottom row) for the land model (left panels) and the seafloor model (right panels). The logarithms of the apparent resistivities are normalized by the logarithms calculated for a flat interface, and the phases are normalized by computing the difference from the absolute values of the phases derived from a flat interface. Results derived for the upper (black lines) and lower (grey lines) region show good agreement on the interface. Deviations are visible in the TM mode phases on the seafloor. While the phase in the lower region shows no influence of the topography, the solution for the upper region has clear deviations when the slope of the interface is maximum, a behaviour similar to the TM mode magnetic field in Fig. 3.

On land, the TM mode apparent resistivities are distorted by topography. There is no visible topographic effect in the TM mode phases and in the TE mode data ($\ll$1 per cent). On the seafloor, both modes are clearly affected by topography. TM mode apparent resistivities are smaller below a hill on land and bigger above a seafloor ridge. TM mode phases show no topographic signature apart from the mismatch mentioned above. In contrast to the land case, the TE mode data are clearly distorted in the presence of a topographic seafloor.

3.1.3 Convergence

An error function has been calculated for the TM mode magnetic fields on the seafloor to check the convergence of the solution. We define the root-mean-square (rms) error as

$$\mathrm{rms} = \sqrt{\frac{1}{N}\sum_x \left(\frac{B^1(x) - B^2(x)}{B^2_{\mathrm{flat}}(x)}\right)^2}. \tag{46}$$

B^2_{flat} is the magnetic field in the lower region on a flat seafloor, N is the number of data. In Fig. 5 the rms is plotted versus the order n. The solution converges and a constant error floor of $\sim$0.5 per cent is reached for $n > 3$. No better agreement between field responses from the upper and lower region at the interface can be reached if higher orders in n are considered.

3.2 Parameter tests

3.2.1 Period

Our analytical approach allows us to systematically test the dependence of specific parameters. In Fig. 6 we show TM and TE mode apparent resistivities (top) and phases (bottom) derived from our analytical formulation for a land surface (left panels) and a seafloor (right panels) for

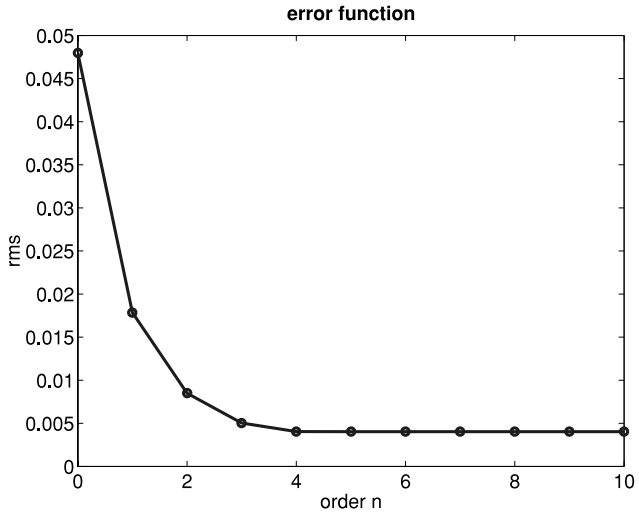

Figure 5. The root-mean-square error calculated for the magnetic field on the seafloor is plotted over order n in Bessel functions. Convergence of the solution is reached for $n > 3$.

Table 2. Approximate induction depths $\delta = 500\sqrt{T/\sigma}$ [m] calculated for the period range $T = 1$–10 000 s. The conductivity σ is 0.01 S m^{-1} and 3 S m^{-1} for the land and the seafloor model respectively.

Period T (s)	Land δ (m)	Seafloor δ (m)
1	5000	290
10	15 800	915
100	50 000	2900
1000	158 000	9150
10 000	500 000	29 000

the period range $T = 1$–10 000 s. TM mode apparent resistivities are frequency independent and phases are constant for both the land surface and the seafloor. Only for $T = 1$ s is a topographic effect visible in the phases which is larger on the seafloor (induction depth $\delta \approx 290$ m) than on land ($\delta \approx 5000$ m, see Table 2). On land, TE mode data are not distorted by topography, as we learned in Section 3.1.2 and Fig. 4, while the data are strongly biased on the seafloor. The smaller the period the larger is the topographic distortion. For the chosen model parameters no periods below 10 s should be applied. However, our analytical approach becomes unstable for $T \leq 0.1$ s, the boundary conditions are not satisfied for all components and the related results are therefore not reliable.

3.2.2 Conductivity contrast

In Fig. 7 we calculated TM and TE mode apparent resistivities and phases for subsurface resistivities between 1 and 10 000 Ω m. The conductivity in the upper region is 10^{-10} S m^{-1} for the land model, and 3 S m^{-1} for the seafloor model. TM mode apparent resistivities show topographic effects for both models. On land, the offset is constant between the respective ρ_a curves according to the changing conductivity contrasts. On the seafloor, the shape of the ρ_a curves flattens the smaller we set the resistivity of the subsurface. This displays the transition from the marine to the land case. If we calculate data on top of a hill, we obtain a decrease in ρ_a if $\sigma_1 < \sigma_2$ and an increase if $\sigma_1 > \sigma_2$. TM mode phases show a negligible topographic effect. Only if $\sigma_2 \leq 1$ S m^{-1} is a bias visible.

As in the previous parameter test, no topographic distortion occurs on land in the TE mode data. Apparent resistivities are constant and the curves are shifted according to the chosen subsurface conductivities. On the seafloor, both TE mode apparent resistivities and phases show topographic effects which become more complex with increasing conductivity contrast. Thereby, the TE mode phases on the seafloor show the same pattern as in the previous parameter test on period dependence. The topographic distortion calculated for a small conductivity contrast for a given period coincides with that derived for a longer period for a given conductivity contrast. A similar behaviour can be found for the TE mode apparent resistivities on the seafloor for a period $T = 1$ s in Fig. 6 and subsurface conductivity $\rho = 10\,000$ Ω m in Fig. 7. In summary, the parameter tests demonstrate that TE mode data are seriously affected by seafloor topography with a strong dependency on the chosen period and conductivity contrast.

3.3 Current streamlines

So far we have shown results calculated on the interface. However, the formulation also enables the calculation of the fields in the entire model. A descriptive presentation is current streamlines which are contour lines of the magnetic field parallel to strike (e.g. Bailey 1977). In

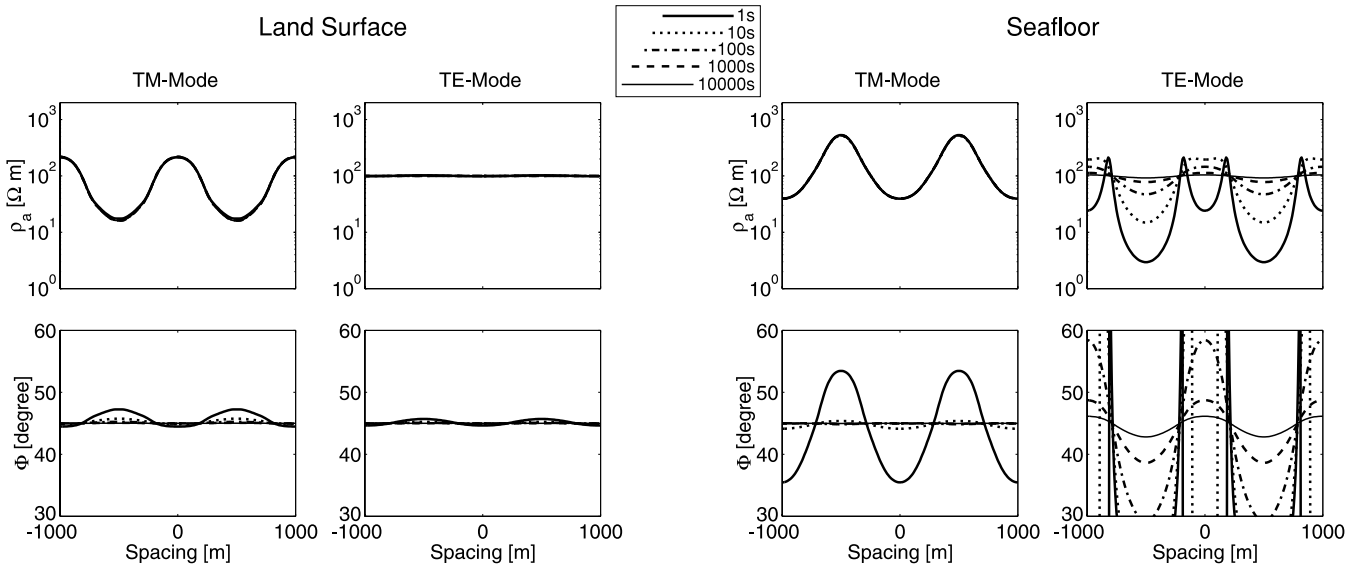

Figure 6. Systematic study to check the period dependence of TM and TE mode apparent resistivities and phases calculated on a land surface and on a seafloor for the period range $T = 1$–$10\,000$ s. TM mode: Apparent resistivities are frequency independent and phases are constant for a wide period range. Phases show a topographic effect for $T = 1$ s which is more pronounced on the seafloor than on land as a result of different induction depths in both cases. TE mode: Topographic effects are negligible on land for the entire range of periods, whereas TE mode data on the seafloor show a strongly frequency-dependent topographic distortion.

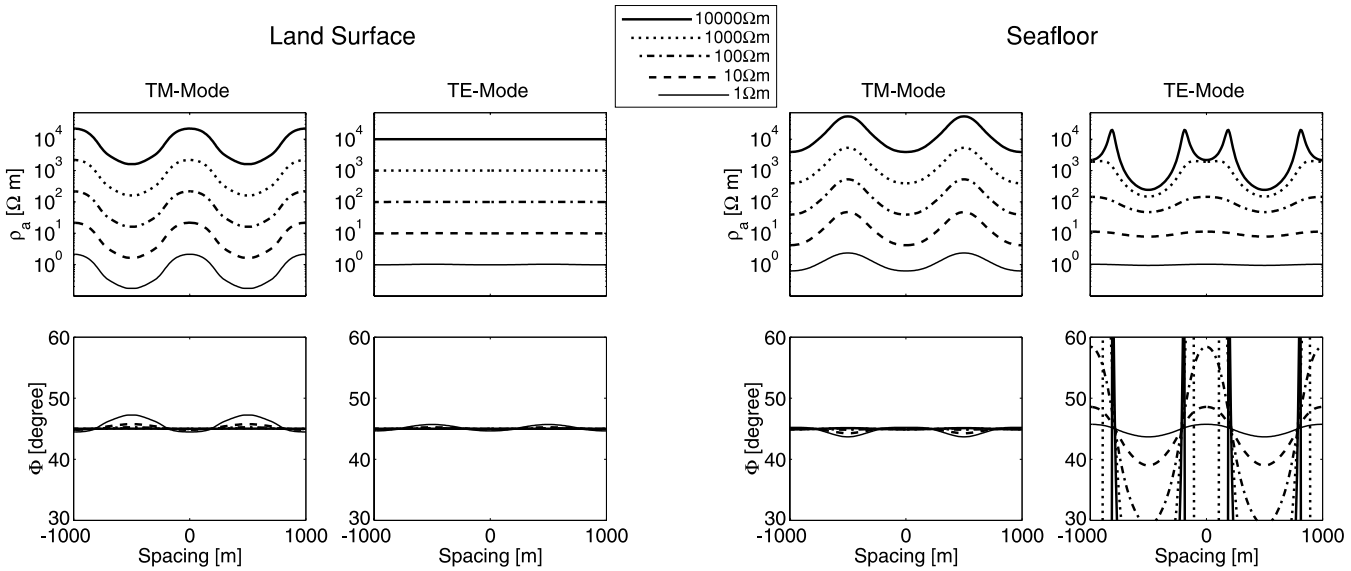

Figure 7. Systematic study to check the dependence on the conductivity contrast of TM and TE mode apparent resistivities and phases for subsurface (left) or sub-seafloor (right) resistivities between 1and 10 000 Ω m. TM mode: Apparent resistivities are shifted with increasing conductivity contrast. On the seafloor the reversal from the marine case to the land case becomes visible with decreasing conductivity contrast. Phases remain almost constant. TE mode: Land data are not affected by topography, apparent resistivities are shifted. Seafloor data strongly depend on the conductivity contrast.

Fig. 8 we show current streamlines for a flat (left) and a sinusoidal (right) land surface. No currents are induced in the non-conductive air. In the absence of topography the streamlines are horizontal and follow the interface. In the presence of topography the streamlines likewise follow the interface, but they diverge below a hill and converge below a valley. This behaviour is identical with a decrease in current density in the related electric field, and subsequently in the apparent resistivity below a hill. Consequently, we observe an increase in current density, electric field and in the apparent resistivity below a valley on land (compare Fig. 4 left, and Chouteau & Bouchard 1988).

In Fig. 9 we show current streamlines for a flat (left) and a sinusoidal (right) seafloor. As expected, the electric currents mainly propagate in the conductive sea layer, i.e. no streamlines are visible in the subsurface region for the chosen conductivity contrast. In the case of a flat seafloor the contour lines are parallel to the interface. In the case of a sinusoidal seafloor we observe converging contour lines above a hill

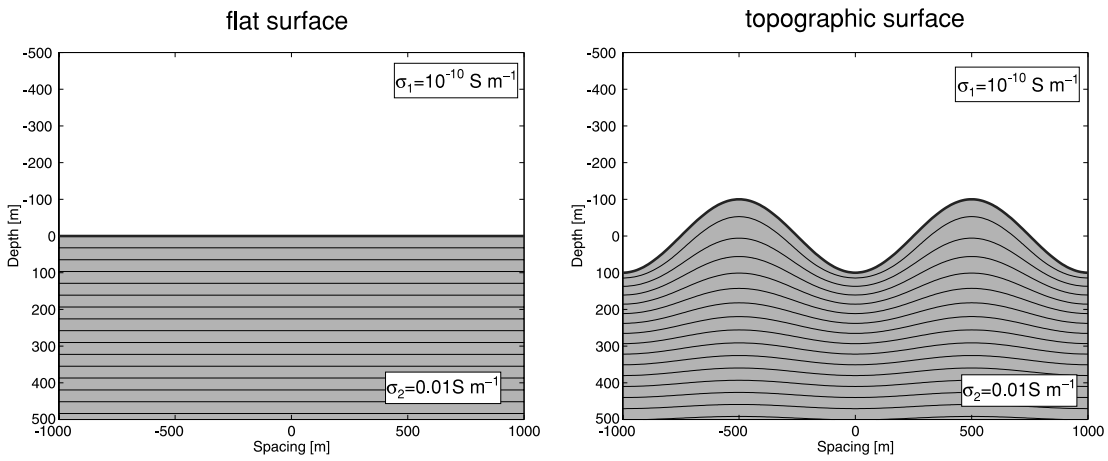

Figure 8. Current streamlines for the land model follow the shape of the flat (left) or sinusoidal (right) surface. On land, a topographic hill causes a decrease in current density j, and subsequently in the electric field E, impedance Z and apparent resistivity ρ_a. In contrast, a topographic valley generates an increase in j, E, Z and ρ_a (see Fig. 4, left).

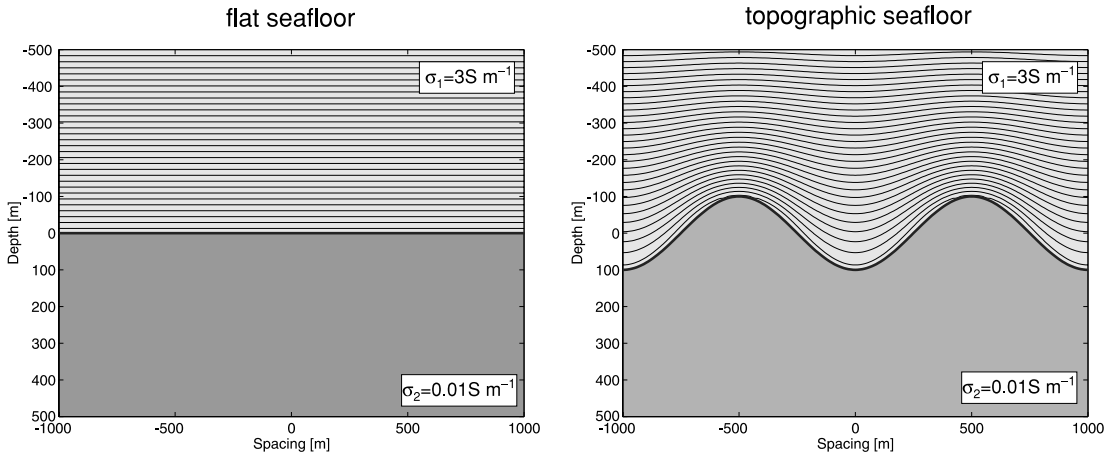

Figure 9. Current streamlines for the seafloor model follow the shape of the flat (left) or sinusoidal (right) surface, but different from the behaviour on land shown in Fig. 8 the currents flow now mainly in the conductive sea layer. In this case, a topographic hill causes an increase in current density in the sea layer and therefore higher E, Z, ρ_a, while the stream lines diverge above a valley, resulting in lower j, E, Z and ρ_a (see Fig. 4, right).

and diverging contour lines above a valley. This explains an increase in apparent resistivity, if measurements are made on a seafloor elevation and a decrease in ρ_a if the measuring site is in a seafloor depression (compare Fig. 4, right).

From Fig. 9 it is not clear whether the TM mode magnetic fields penetrate into the lower region. In Fig. 10 we used a model with a conductivity contrast of 1/5. Now it is obvious that the current streamlines are continuous at conductivity contrasts. Current density is less in the lower region and the main part of the exciting external field has been absorbed by the more conductive upper layer. The sketch in the right part of Fig. 10 demonstrates the behaviour of the field lines at a discontinuity. The incident field in the conductive upper region arrives at the interface under angle α_1, and is transmitted in the more resistive lower region under angle $\alpha_2 < \alpha_1$.

Contour lines of the remaining MT fields (E_{TE}, E_{TM}, B_{TE}) can be calculated from the analytical formulation. However, these quantities are physically less instructive, and are not shown here.

4 NUMERICAL RESULTS

In this section we compare field responses calculated from a discrete model with the analytically obtained results in the preceding section. We used the 2-D forward code by Wannamaker (1990) to design a model with a topographic interface similar to the sinusoidal interface in Fig. 1. In Fig. 11, we show current streamlines for a discrete model that is defined by the same parameters as given in Table 1. Qualitatively, the results show the same behaviour as the analytically obtained result in Fig. 9 (right). In the vicinity of the interface between sea water and seafloor the contour lines are deformed by the interface and return back to their horizontal direction with decreasing water depth. No contour lines appear in the lower region for the chosen conductivity contrast. The numerical approach also enables us to make quantitative considerations. We added labels to the contour lines, and normalized them by the surface value. For the given model the normalized field values on the seafloor decay to ∼1/10 of their values on the sea surface. We also calculated current streamlines for periods $T = 10$ s and

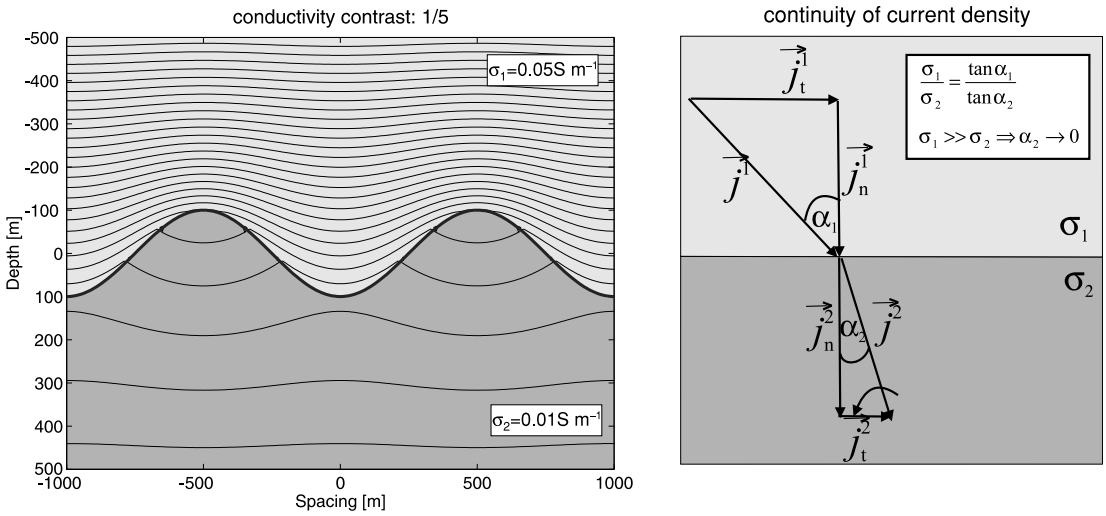

Figure 10. Left: Current streamlines of B_y for a model with a conductivity contrast of 1/5. Contour lines are now visible in the upper and lower region. Current density is less in the resistive region. The streamlines are transmitted under angle $\alpha_2 < \alpha_1$ in the more resistive region as demonstrated in the sketch in the right figure.

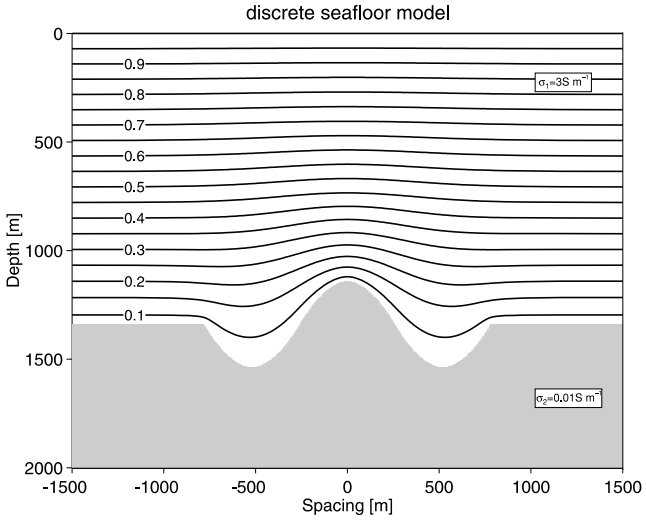

Figure 11. Discrete seafloor model with a topography similar to the sinusoidal interface in Fig. 9. Current streamlines calculated with Wannamaker's 2-D code follow the shape of the interface and show the same behaviour as derived from the analytical formulation. On the seafloor the fields drop to ∼1/10 of their values on the sea surface for the chosen model.

$T = 1000$ s. They show the same qualitative behaviour as for $T = 100$ s, but decay to ∼1/50 for the smaller period and to ∼1/5 for the larger period. This behaviour is consistent with an increasing induction depth with increasing period.

With the numerical approach we are more flexible regarding model design. This motivated us to modify the seafloor model in Fig. 11 into a coast model, shown in Fig. 12. The current streamlines derived from this model follow the shape of the seafloor. Near the coast, the continuity of current density forces the field lines to enter the resistive crust where they penetrate deeply into the crust, following the law of refraction outlined in Fig. 10 (right). Normalized field line values show they decay to ∼1/5 of their surface value close to the coast. They decline to smaller values outside the displayed model part. On a larger scale the field lines also return to a horizontal direction, which is not clear from Fig. 12.

We finally present an example from the Central Andes. The resistivity model in Fig. 13 is the outcome of the 2-D inversion of MT data along an east–west striking profile at 21°S and has been discussed in detail by Brasse *et al.* (2002). The main feature of the model is a huge conductivity anomaly in the backarc below the Altiplano (the Altiplano conductor). The model is also characterized by a resistive forearc, a localized conductor below the West Fissure, a large fault system in the forearc, and high resistivities below the arc volcanoes.

The TM mode magnetic field has been calculated for this entire model using the algorithm of Wannamaker (1990). In Fig. 13 (upper three panels) current streamlines have been derived for periods $T = 100$, 1000 and 10 000 s, and are superimposed on the resistivity model. First, it is visible how the current system penetrates deeper into the subsurface with increasing period. Plotting labels of normalized field values on the contour lines supports this behaviour. Secondly, some details can be seen. For period $T = 100$ s most of the contour lines are

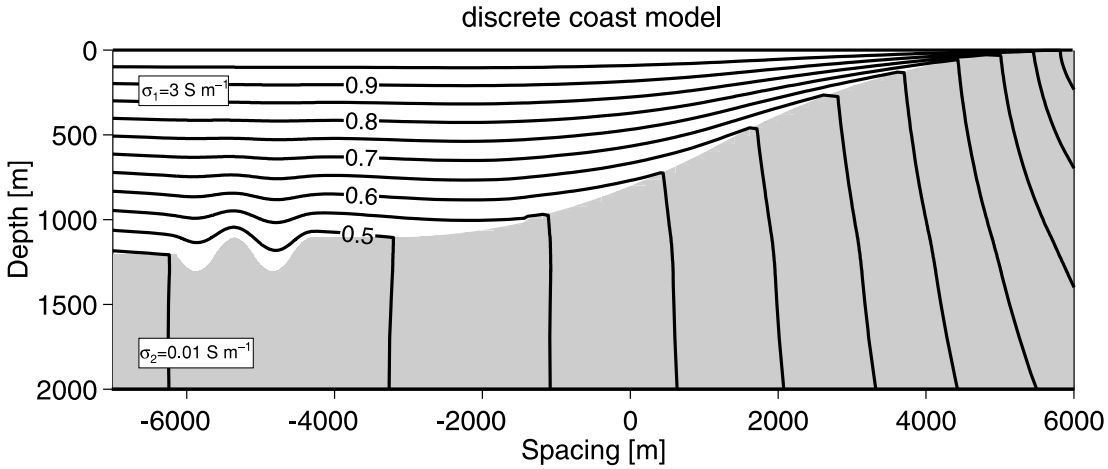

Figure 12. Fig. 11 has been extended toward a coast model. Current streamlines are horizontal in the sea layer and follow the shape of the interface. At the coast they are refracted in the resistive crust. Notice the vertical exaggeration.

channelled in the conductive sediments covering the forearc crust. Few contour lines penetrate deeply into the forearc. This is in agreement with the behaviour we have already seen for the discrete coast model in Fig. 12. Furthermore it can be seen that the contour lines are affected by the localized conductor below the West Fissure in the forearc. In the backarc, the field lines are trapped in the upper part of the Altiplano conductor for $T = 100$ and 1000 s. This effect is minor for $T = 10\,000$ s.

These results are consistent with the outcome of sensitivity studies by Schwalenberg *et al.* (2002). For comparison we show isolines of averaged sensitivities in the lowest panel in Fig. 13. These studies show that the poor sensitivity below the resistive forearc is likely due to the presence of a deep trench in the Pacific Ocean, which restricts the electric currents from reaching greater depths in the forearc crust. The studies also arrive at the conclusion that the lower boundary of the Altiplano anomaly cannot be resolved from the obtained data, a result that can be supported by the current streamline images by the higher density of field lines in the upper part of the anomaly. Regarding the localized conductor below the West Fissure, this has been a well-resolved feature in all sensitivity studies and obviously affects the electric current pattern perpendicular to strike.

5 CONCLUSIONS AND OUTLOOK

In this paper we have shown that it is possible to find an analytical formulation to describe seafloor topography. Our basic model is a sinusoidal interface separating a conductive sea layer from a resistive crust. For comparison we also applied the approach to a land model with the same curvature. The central element of our formulation is a system of linear equations to solve for two sets of unknown coefficients β_n and γ_n. This requires the composition of a $2n \times 2n$ matrix containing terms of modified Bessel function, the most difficult part of the whole derivation. A new aspect is that our formulation does not need any perturbation procedures to give reasonable results, an issue that restricted former approaches to treat moderate topography and/or limited conductivity contrast (e.g. Mann 1964; Geyer 1970; Hughes 1973). The only approximation we make is a simplification of the boundary condition of the electric field at the interface. Instead of the tangential component we require the horizontal component to be continuous across the interface, an approximation that is applicable if the amplitude/wavelength ratio does not exceed 1/10. The approximation can be removed if steeper gradients are encountered.

We can calculate electric and magnetic field responses and impedances on the interface to demonstrate the validity of the boundary condition, and to show TM and TE mode characteristics for a land and a seafloor model. On land, only TM mode fields and impedances are affected by topography; no distortion occurs in the TE mode data. The TM mode magnetic field depends on the external source field and is not affected by subsurface structure or topography. Topographic distortion occurs in the TM mode electric field and in the TM mode apparent resistivities. The quantities are smaller on a hill and larger in a valley. On the seafloor, both TM mode and TE mode data are affected by topography, with the exception of the TE mode electric field which displays a negligible topographic effect. The TM mode magnetic field is consistently reduced by the sea layer. Seafloor topography causes an additional reduction effect, but the effect depends little on the curvature. TM mode electric fields and apparent resistivities are increased on seafloor topographic highs and reduced in a depression.

Useful insight into the physical behaviour inside the model is provided by plotting current streamlines which are contour lines of the TM mode magnetic field. For the land model, the contour lines diverge below a hill and converge below a valley, explaining the behaviour of TM mode electric fields and apparent resistivities at the surface. For the seafloor model, electric currents mainly flow in the conductive sea layer. Contour lines show the opposite behaviour to the land model: divergence above a seafloor depression and convergence above a ridge, explaining the respective TM mode electric fields and apparent resistivities on the seafloor.

These results have been compared with numerically obtained results. We composed a seafloor model with similar topography and calculated the TM mode magnetic field using Wannamaker's 2-D forward code (Wannamaker 1990). The contour plots are in agreement with the analytical solution. Numerical approaches are more flexible than analytical ones with regard to the complexity of the topography and

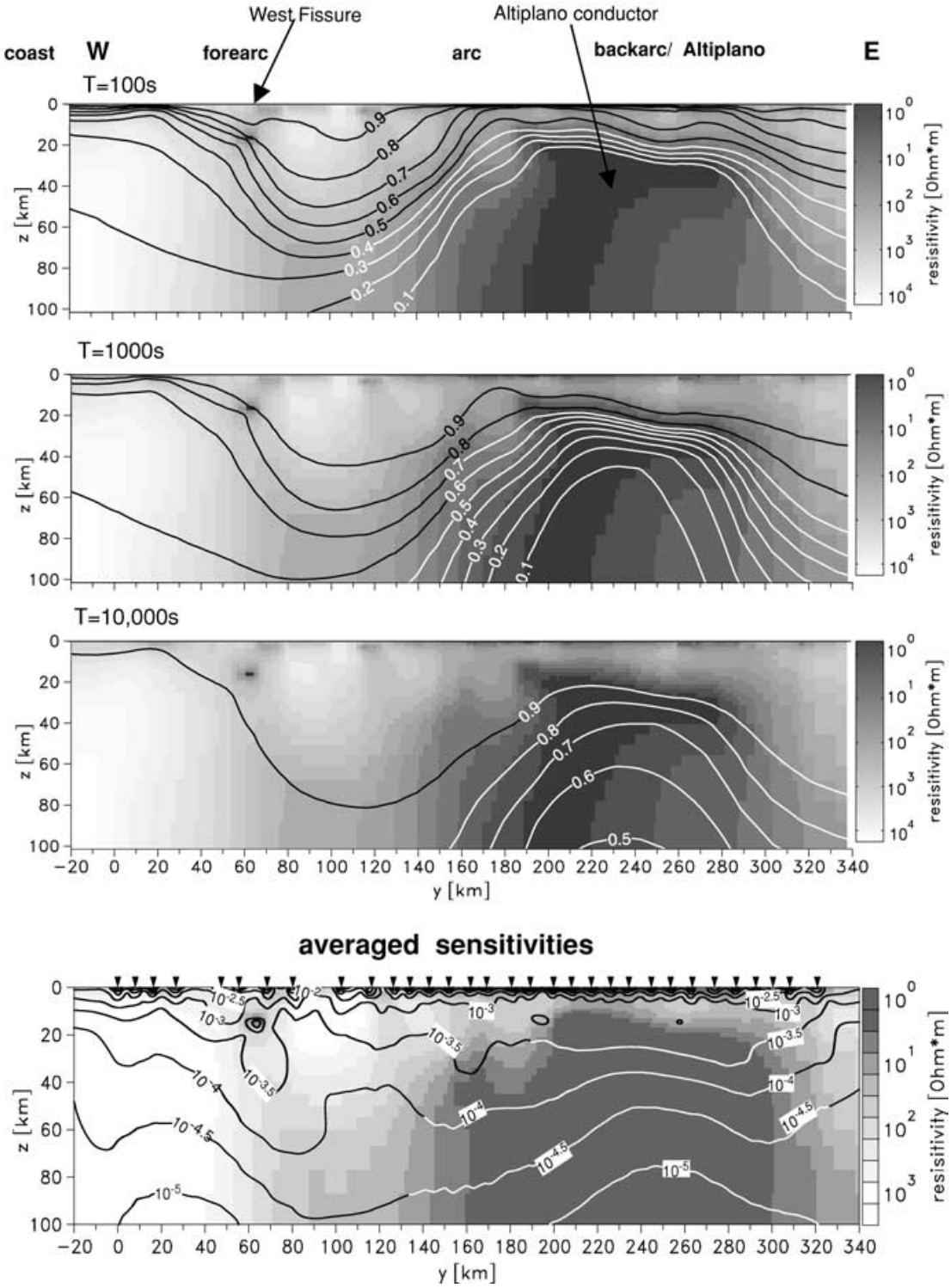

Figure 13. Resistivity model from the Central Andes. The upper three panels show current streamlines for periods $T = 100$, 1000 and 10 000 s. The current systems cover deeper model parts with increasing period. Near the coast, the contour lines dive deeply in the resistive forearc. They are biased by a localized conductivity anomaly below the West Fissure, a large north–south striking fault system. The backarc is dominated by a huge conductivity anomaly (Altiplano conductor). For $T = 100$ s and 1000 s the current streamlines are trapped in the upper part which is coincident with an unresolved depth extent of that structure. Isolines of averaged sensitivities by Schwalenberg *et al.* (2002) are shown in the lower panel for the same resistivity model. Differences in the models are due to different colour scales in the plotting routines. Low sensitivity below the forearc coincides with a smaller density of current streamlines and high sensitivity below the Altiplano coincides with high density of current streamlines in the upper part of the Altiplano conductor.

subsurface conductivity distribution that can be treated. As an application we showed electrical streamlines for a coast model and a model from the Central Andes. In the first example the contour lines are refracted at the sea water/crust interface and dive deeply into the crust before they return to their horizontal direction far away from the contrast. The second example confirms the outcome of sensitivity studies by Schwalenberg *et al.* (2002) which show lower sensitivity below the forearc close to the Pacific coast and higher sensitivity in the upper, well-resolved part of a huge conductivity anomaly in the backarc crust. We think that these results demonstrate the utility of examining current streamlines when discussing the physical details of a model.

Our analytical solution for seafloor topography can be compared with numerical results which generally have large instabilities at the seafloor interface. However, a number of unresolved problems arise from our approach:

(1) A sinusoidal interface may not represent geological reality. Theoretically, it should be possible to express any arbitrary seafloor curvature by a Fourier series of the form

$$z(x) = \sum_{m=0}^{\infty} a_m \cos(mx). \tag{47}$$

In practice, the derivation of a system of linear equations becomes very complex and intractable. In our formulation, the expressions which define the interface are considered in a non-linear way. Reasonable approximations or a different approach must be found to consider more complicated interfaces.

(2) For a general solution it is still required to consider the vertical electric field in the TM mode formulation.

(3) A major goal behind our formulation is to find a correction method to remove the topographic effects directly from the data. This requires that the measured impedance can be decomposed in a term containing subsurface information and a term which only depends on topography:

$$Z^{\text{measured}} = f(Z^{\text{earth}}, Z^{\text{topo}}).$$

This has been solved by Chouteau & Bouchard (1988) for different land surfaces when topographic distortion mainly affects the TM mode electric field, but their method cannot be transferred to the seafloor case when distortion occurs in both modes and in the electric and magnetic fields. However, our results are helpful for understanding the physics of electromagnetic field behaviour in both the land and marine case, and should be deemed to be a starting point for future work.

ACKNOWLEDGMENTS

We thank Rob Evans, an anonymous reviewer, Martyn Unsworth, Kiyoshi Baba and Misac Nabighian for their thoughtful reviews and commentaries. Phil Wannamaker supplied his 2-D finite-element code. Kerry Key provided a MATLAB script to plot streamlines for numerical models. The project in general and KS in particular have been supported by a grant from the Natural Sciences and Engineering Research Council of Canada.

REFERENCES

Aprea, C., Booker, J.R. & Smith, J.T., 1997. The forward problem of electromagnetic induction: accurate finite-difference approximations for two-dimensional discrete boundaries with arbitrary geometry, *Geophys. J. Int.,* **129**, 29–40.

Baba, K., 2002. Topograhic correction of seafloor magnetotelluric data using flattening surface modeling, *16th Workshop on Electromagnetic Induction on the Earth, 16–22 June 2002, Santa Fe, New Mexico, USA,*

Baba, K. & Seama, N., 2002. A new technique for the incorporation of seafloor topography in electromagnetic modelling, *Geophys. J. Int.,* **150**, 392–402.

Bailey, R., 1977. Electromagnetic induction over the edge of a perfectly conducting ocean: the H-polarization case, *Geophys. J. R. astr. Soc.,* **48**, 385–392.

Brasse, H., Lezaeta, P., Rath, V., Schwalenberg, K., Soyer, W. & Haak, V., 2002. The Bolivian Altiplano conductivity anomaly, *J. geophys. Res.,* **107**(B5), 10.1029/2001JB000391.

Chouteau, M. & Bouchard, K., 1988. Two-dimensional terrain correction in magnetotelluric surveys, *Geophysics,* **53**, 854–862.

Geyer, R., 1970. The effect of subsurface geological structure in electromagnetic induction prospecting, *PhD thesis,* Thesis 1307, Colorado School of Mines, Golden, CO.

Gradshteyn, I.S. & Ryzhik, I.M., 2000. *Table of Integrals, Series, and Products,* 6th edn, Academic Press, New York.

Hughes, W., 1973. The effect of two periodic conductivity anomalies on geomagnetic micropulsation measurements, *Geophys. J. R. astr. Soc.,* **31**, 407–431.

Jegen, M.D., 1997. Electrical properties of the mantle upwelling zone beneath a mid ocean ridge, an application of vertical gradient sounding, PhD thesis, Department of Physics, University of Toronto.

Jiracek, G., Reddig, R. & Kojima, R., 1989. Application of the Rayleigh-FFT technique to magnetotelluric modeling and correction, *Phys. Earth planet Inter.,* **53**, 365–375.

Mann, J., 1964. Magnetotelluric theory of the sinusoidal interface, *J. geophys. Res.,* **69**, 3517–3524.

Nolasco, R., Tarits, P., Filloux, J. & Chave, A., 1998. Magnetotelluric imaging of the Society Islands hotspot, *J. geophys. Res.,* **103**(B12), 287–309.

Rikitake, T., 1965. Electromagnetic induction in a semi-infinite conductor having an undulatory surface, *Bull. Earthquake Res. Inst.,* **43**, 161–166.

Schwalenberg, K., Rath, V. & Haak, V., 2002. Sensitivity studies applied to a 2-D resistivity model from the Central Andes, *Geophys. J. Int.,* **150**(3), 673–686.

Smith, J.T. & Booker, J.R., 1988. Magnetotelluric inversion for minimum structure, *Geophysics,* **53**, 1565–1576.

Wannamaker, P.E., 1990. *PW2D—Finite Element Programme for Magnetotelluric Forward Modeling and Parameterized Inversion of Two-dimensional Earth Resistivity Structure,* User documentation, University of Utah Research Institute Earth Science.

Wannamaker, P.E., Stodt, J.A. & Rijo, L., 1986. Two-dimensional topographic responses in magnetotelluric models using finite elements, *Geophysics,* **51**(11), 2131–2144.

Zhdanov, M.S. & Keller, G.V., 1994. *The Geoelectrical Methods in Geophysical Exploration,* Elsevier, Amsterdam.